Research Article   **Open Access**

Andrzej Truty*

On consistent nonlinear analysis of soil–structure interaction problems

Abstract: Nonlinear soil–linear structure computational strategy is commonly accepted in the community of geotechnical engineers using advanced finite element software for solving complex soil–structure interaction problems. However, further design procedure of the structural elements is carried out using increased values of the computed elastic stress resultants. It is absolutely not clear whether this method is conservative and, therefore, whether safe or not. To tackle this problem, a fully consistent nonlinear analysis of a deep excavation protected by the diaphragm wall is analysed here. The subsoil is modelled using the Hardening Soil model, while reinforced concrete is modelled using the modified Lee–Fenves model enhanced by the Eurocode 2 (EC2)-compatible creep module, developed by the author. It is shown that the commonly used nonlinear soil–linear structure computational strategy may yield insufficient amount of reinforcement from the ultimate limit state (ULS) and serviceability limit state (SLS) points of view. A consistent and conservative method of combining fully nonlinear analysis and the rules imposed by the EC2 is proposed.

Keywords: soil–structure interaction; constitutive modelling; deep excavations; finite elements.

1 Introduction

In most of the finite element (FE) simulations, carried out for certain classes of soil–structure interaction problems, such as deep excavations, a computational strategy that assumes nonlinear soil and linear structure (NSO–LST) behaviour is usually adopted. Such an approach should lead to the conservative assessment of stress resultants in the structure, and a safer design in consequence, but it is rather difficult to say whether this hypothesis holds true in all cases. The main source of this uncertainty is because most of the structural design methods are based on preliminary linear elastic computations, then dimensioning of the structural members based on dedicated standards, and finally checking the serviceability limit states (SLSs). The main role of advanced FE modelling is rather to check the SLSs using global analysis. A fully consistent approach in which both subsoil and structure are treated as nonlinear materials, including visco-elastic creep, in the structure, is proposed and analysed in this paper. A similar approach was recently analysed by Obrzud et al. [1]; however, the concrete model used in their study was strictly limited to the 1D stress–strain representation, and the applied creep law was not compatible with the Eurocode 2 (EC2) standard. When we analyse statically undetermined systems, consisting of subsoil and structure, it is well known that internal force distribution depends on the relative stiffness of the two model components. Diaphragm walls are good representatives of the considered problem. In the case of deep excavations the resulting bending moments, in certain zones of the wall, are usually larger than the cracking moment. Therefore, cracks must occur and the overall stiffness of the structure is reduced. In consequence, the role of the adjacent subsoil in these zones becomes important. A selected case study of the diaphragm wall designed and constructed in the Supersam project in Warsaw (Poland) [2] is analysed in this paper. For the sake of simplicity, a uniform quaternary sandy clay layer is considered in the subsoil, modelled using the commonly accepted Hardening Soil (HS) model with small strain overlay, while the diaphragm wall is modelled using the modified plastic-damage model, developed by Lee and Fenves [3, 4]. The latter model is implemented by the author in the ZSoil software, in the modified form that includes creep and ageing [5]. The paper is organised as follows. A short description of the HS model used to represent the subsoil behaviour is given in Section 2. Rheological aspects and implementation details of the modified Lee–Fenves model for concrete are given in Section 3. The diaphragm

*Corresponding author: Andrzej Truty, Instytut Geotechniki, Wydział Inżynierii Środowiska, Politechnika Krakowska, E-mail: andrzej.truty@pk.edu.pl

wall case study based on the data collected from the Supersam project [2] is described and analysed in Section 4. In the two subsections of the aforementioned section, two computational strategies, i.e. nonlinear soil–linear structure (NSO-LST) and then nonlinear soil–nonlinear structure (NSO-NST) are analysed. Final conclusions are drawn in Section 5.

2 Modelling subsoil behaviour

The HS model worked out by Schanz, Vermeer and Bonnier [6, 7], extended later to the domain of small strain stiffness by Benz [8], is frequently used in global analyses of deep excavations. It has proved to be very useful and predictive in many practical cases all over the world. It has also some certain drawbacks such as unlimited shear strength for soils exhibiting dilatant behaviour in shear, but also $\sigma_3^{'}$ based stress dependency in definitions of the initial and the unloading–reloading stiffness moduli. Problems with the unlimited shear strength appear at larger strains, which is not the case in the considered class of problems, unless the global ultimate limit state (ULS) is analysed; however, this problem can easily be removed by coupling the shear and volumetric mechanisms in the model, as shown by Truty and Obrzud [9]. The second aforementioned model deficiency is important in the case of cohesionless soils, where $p^{'}$, the stiffness stress dependency, represents soil behaviour in a definitely more accurate manner. This is so because, for sandy soils, in most cases, we assume the in situ earth pressure coefficient $K_o = K_o^{NC}$. By using $p^{'}$ stiffness stress dependency in the HS model, the excessive heaving of the bottom of excavations is always smaller than in the case when $\sigma_3^{'}$ stress dependency is used. The complete theory of the model, implemented in the ZSoil software, with all introduced modifications, can be found in the detailed report written by Obrzud and Truty [10]. It has to be emphasised here that most of the HS model parameters have clear physical interpretations, and model calibration can be made using standard triaxial consolidated drained (CD) or consolidated undrained (CU) test, including shear wave velocity measurement, and oedometer test. The latter one is used to assess the oedometric tangent stiffness modulus (on primary consolidation line), at a given reference stress, but also the pre-consolidation pressure. It is usually recommended to verify the preconsolidation pressure using in situ tests such as seismic cone penetration test (SCPTU) or seismic dilatometer test (SDMT). This combination of laboratory and in situ tests is the key to obtaining high-quality

predictions when analysing complex practical problems. One should also mention that all samples tested in the triaxial apparatus should be overconsolidated and at least one unloading–reloading cycle should be carried out to assess precisely the reference unloading–reloading stiffness modulus E_{ur}^{ref}. In the case of overconsolidated samples, the shear and volumetric mechanisms in the HS model become uncoupled and the secant stiffness parameters E_{50}^{ref} can easily be determined (see Fig. 1). The last important aspect concerns the assessment of the overconsolidation ratio $(OCR)(z)$ profile, which is needed to initialise the internal state parameters, i.e. the size of the elliptic surface representing the volumetric plastic mechanism and the position of the current yield surface representing the shear plastic mechanism, of the HS model. It is worth underlining that for shallow subsoil layers, setting a unique OCR value does not represent the real in situ conditions. The OCR profile is a highly nonlinear function of depth (see Fig. 2), and its definition through the value of the pre-overburden pressure is more accurate. Knowledge on the current in situ effective stress state and the OCR value, at a given point in the subsoil, has to be sufficient to make this setting. In the case of multisurface plasticity, the intersection point σ^{SR} (see Fig. 3) of the two plastic surfaces plays the role of stress attractor. It means that in the past history, an effective stress state was present in the vicinity of this position. If we assume that the historical σ^{SR} stress state corresponds to the K_o^{NC} state, then it can be expressed as follows:

$$\sigma_z^{SR} = \sigma_z^o \, OCR$$
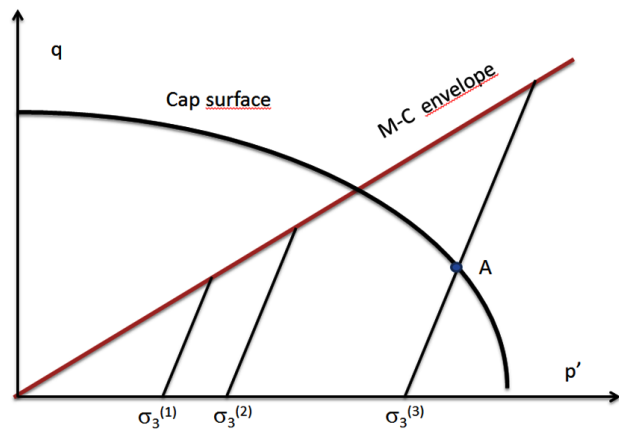$$\sigma_x^{SR} = \sigma_y^{SR} = K_o^{NC} \, \sigma_z^{SR} \tag{1}$$

Figure 1: Problem of coupling shear and volumetric plastic mechanisms during triaxial CD test carried out on normally or lightly overconsolidated samples.
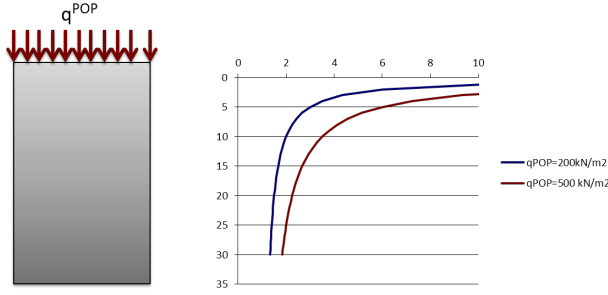
Figure 2: OCR profiles for assumed pre-overburden pressure values q^{POP}.
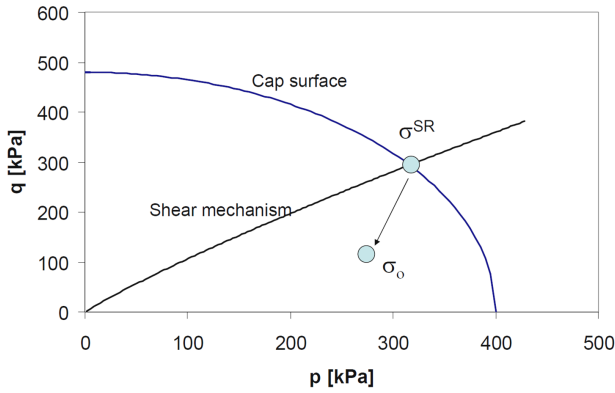

Figure 3: Setting the initial position of the plastic surfaces of the HS model.

3 Modelling concrete behaviour using the modified Lee–Fenves model

The Lee–Fenves concrete plastic-damage model (CPDM) [3] , in which several ingredients of the Barcelona model, developed earlier by Lubliner et al. [11], and then by Oller et al. [12], are exploited, becomes one of the most frequently used in nonlinear analyses of plain and reinforced concrete (RC) structures. In this relatively simple model, implemented in the computer FE codes such as Abaqus and ZSoil, two independent damage variables are used, one for the tensile damage and one for the compressive damage. In the ZSoil code, a modified version of the model was implemented by the author. The main modifications concern the yield surface description, delay of damage and dilatancy with respect to the onset of plastic straining and the EC2-compatible ageing, creep and fire extensions. The presence of elastic stiffness degradation and stiffness recovery in cyclic tension–compression tests (partial closure of cracks) is the main benefit of this model, formulated in the framework of a

coupled continuum damage and plasticity, and assuming the so-called strain equivalence between the nominal and effective stress configurations (effective stresses in this model have nothing to do with the classical notion of effective stresses known in soil mechanics). All details concerning the reference CPDM model are given in papers [3, 4], and the modified version (without creep and ageing), implemented in the ZSoil code, is described by Truty and Zimmermann [13]. Due to the limited scope of the paper, only creep and ageing extensions of the model are presented here, while the complete theory and implementation schemes can be obtained from the aforementioned publications.

3.1 Adding EC2-compatible visco-elastic creep to the model

The CPDM model can be extended to capture the visco-elastic creep and ageing based on the EC2 standard. To simplify the formulation, nonlinear creep effects that may appear for larger compressive stresses are neglected, and no distinction is made between the creep effects in compression and tension. In the EC2 standard, creep and ageing are represented by the creep coefficient $\phi(t,t_o)$, understood as a ratio between the creep and an instantaneous elastic strain computed for concrete loaded at t=28 days, and defined as follows:

$$\phi(t,t_o) = \phi_o \beta_c(t,t_o) \tag{2}$$

where

$$\phi_o = \phi_{RH} \beta(f_{cm}) \beta(t_o) \tag{3}$$

$$\phi_{RH} = \begin{cases} 1 + \dfrac{1 - \dfrac{RH}{100}}{0.1\, h_o^{1/3}} & \text{for} \quad f_{cm} \leq 35\text{MPa} \\[4mm] \left(1 + \dfrac{1 - \dfrac{RH}{100}}{0.1\, h_o^{1/3}} \alpha_1 \right) \alpha_2 & \text{for} \quad f_{cm} > 35\text{MPa} \end{cases} \tag{4}$$

$$\beta(f_{cm}) = \frac{16.8}{\sqrt{f_{cm}}} \tag{5}$$

$$\beta(t_o) = \frac{1}{0.1 + t_o^{0.2}} \tag{6}$$

$$\beta_c(t,t_o) = \left[\frac{t - t_o}{\beta_H + t - t_o} \right]^{0.3} \tag{7}$$

$$\beta_H = \begin{cases} \min\!\left(1.5\left[1 + (0.012 RH)^{18}\right] h_o + 250, 1500\right) & \text{for} \quad f_{cm} \leq 35\text{MPa} \\ \min\!\left(1.5\left[1 + (0.012 RH)^{18}\right] h_o + 250\alpha_3, 1500\alpha_3\right) & \text{for} \quad f_{cm} > 35\text{MPa} \end{cases}$$

(8)

In these expressions, $\alpha_1 = (35/f_{cm})^{0.7}$, $\alpha_2 = (35/f_{cm})^{0.2}$, $\alpha_3 = (35/f_{cm})^{0.5}$; the relative humidity RH is expressed in percentage, the equivalent member size h_o is expressed in millimetre, an averaged compressive strength f_{cm} is expressed in megapascals and the loading time t_o is expressed in days. The implementation scheme, in which the creep curve is approximated by a set of non-ageing Kelvin units, is partially based on the implicit algorithm proposed by Havlásek [14]. To eliminate the time dependency of Kelvin units, the amplitude A_μ (in the ageing material) of the current creep strain increment (see Eq. 9) is divided by a factor v^{cr}, which amplifies, at early stages, or reduces, for old concrete, the current creep rate. Therefore, the increment of the current creep strains is expressed as follows:

$$\Delta\boldsymbol{\varepsilon}_{n+1}^{cr} = \mathbf{D}_o^{-1} \frac{1}{v_{n+1/2}^{cr}} \sum_{\mu=1}^{N} A_\mu \left(1 - \beta_{\mu,n+1}\right) \boldsymbol{\sigma}_{v\mu,n} \qquad (9)$$

In the above expression, the visco-elastic projection matrix is denoted by $\mathbf{D}_o^{-1} = E_{28}\,\mathbf{D}^{-1}$, $v_{n+1/2}^{cr}$ is an extra scaling factor amplifying the creep rate due to the ageing phenomenon, $\boldsymbol{\sigma}_{v\mu,n+1}$ represents the viscous effective stresses in the $\mu-th$ Kelvin unit (number of Kelvin units in the chain is denoted by N), the algorithmic factor $\beta_{\mu,n+1} = \exp(-\Delta t_{n+1}/\tau_\mu)$, the retardation time of μ-th Kelvin unit is denoted by τ_μ and the ultimate creep strain value for the μ-th Kelvin unit, obtained for unit stress, is denoted by A_μ.

The following updated procedure for the viscous stresses, in each Kelvin unit, is used:

$$\boldsymbol{\sigma}_{v\mu,n+1} = \beta_{\mu,n+1}\boldsymbol{\sigma}_{v\mu,n} + \lambda_{\mu,n+1}\Delta\overline{\boldsymbol{\sigma}}_{n+1} \qquad (10)$$

The algorithmic term $\lambda_{\mu,n+1}$ is equivalent to $\lambda_{\mu,n+1} = (1-\beta_{\mu,n+1})\frac{\tau_\mu}{\Delta t_{n+1}}$, while $\Delta\overline{\boldsymbol{\sigma}}_{n+1}$ represents the stress increment in effective (undamaged) configuration at any integration point in the structure. Assuming that the structure is loaded after 28 days, the algorithmic effective Young's modulus is expressed as follows:

$$E = \frac{1}{\dfrac{1}{E_{28}} + \dfrac{1}{v^{cr}}\displaystyle\sum_{\mu=1}^{N}\left(1-\lambda_{\mu,n+1}\right)A_\mu} \qquad (11)$$

The v^{cr} term appearing in Eq. 9 and Eq. 11 can be derived based on the following reasoning. Evolution of the creep strain in time, according to EC2, is expressed by the following equation:

$$\varepsilon^{cr} = A_1\left(\frac{t-t_o}{\beta_H + t - t_o}\right)^{0.3}\beta(t_o) \qquad (12)$$

where $A_1 = \phi_{RH}\beta(f_{cm})/E_{28}$, while $t-t_o$ is the time of creeping. Let us now introduce the reference creep strain curve corresponding to the loading time $t_o = 28$ days:

$$\varepsilon_{ref}^{cr} = A_1\left(\frac{t-t_o}{\beta_H + t - t_o}\right)^{0.3}\beta(t_o = 28) \qquad (13)$$

where $t-t_o$ is also the time of creeping. This reference curve is approximated by the chain of Kelvin elements in which the retardation times τ_μ are adjusted with respect to the predicted time of analysis to be carried out. Once the retardation times τ_μ are set, the A_μ coefficients, in the chain of non-ageing Kelvin units, can be optimised using standard optimisation methods. Keeping the amplitudes of Kelvin elements, defined for the reference curve, constant while hiding the ageing effects in the v^{cr} term is the main goal of this approach. To derive the v^{cr} term, we assume the following compatibility condition for the creep strain rates at any creeping time $t-t_o$.

$$\dot{\varepsilon}^{cr} = \frac{1}{v^{cr}}\dot{\varepsilon}_{ref}^{cr} \qquad (14)$$

This yields the following expression for the v^{cr} term:

$$v^{cr} = \frac{\beta(t_o = 28)}{\beta(t_o)} \qquad (15)$$

where t_o is the age of concrete at the beginning of analysis. The proposed simplified approach yields an equivalent, relative to the EC2, visco-elastic implicit creep model.

4 Case study

In order to analyse the consequences of the consistent nonlinear analysis that takes into account the cracking, creep and ageing effects in the RC structure, a deep excavation, carried out in the uniform layer of quaternary sandy clays and protected by a diaphragm wall, is analysed here. This case study was already considered in the author's earlier publication [15], but it was strictly limited to the problem of the in situ stress disturbance caused by the diaphragm wall installation procedure and its influence on the resulting wall deformations. This aspect is neglected in the paper. As the CPDM model can be used in continuum and shell elements only (it cannot be used in a consistent manner in beam elements as, in the ZSoil beam formulation, bending is decoupled from shear [which is treated in a linear manner]), the practical 2D problem is analysed here using one row (in out of plane direction) of Q4 mixed interpolation of tensorial
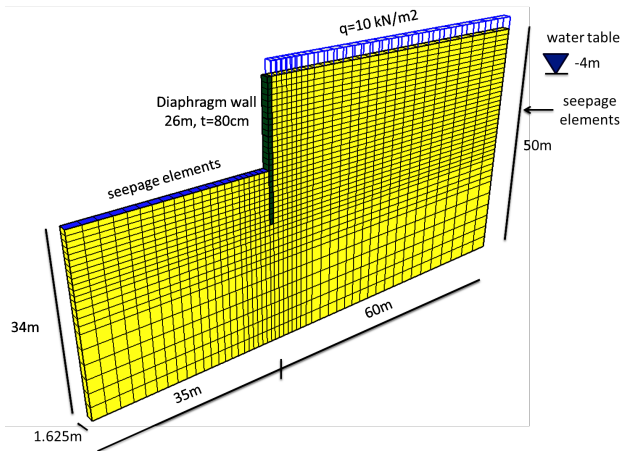
Figure 4: FE model of deep excavation protected with a diaphragm wall.

components (MITC) shell elements, possessing typical brick B8 geometry, representing diaphragm wall, and locking free eight-node enhanced assumed strain (EAS) brick continuum elements to represent subsoil behaviour (see Fig. 4). Frictional Coulomb-type contact interface is placed between the wall and the subsoil, at all stages of the analysis, except the initial state, where the full sticking condition is enforced. Pressure boundary conditions (BCs) consist of the fluid head BC (−4 m) plus seepage elements applied to the right vertical wall of the model but also seepage elements (to represent free-draining condition) activated at the current bottom of the excavation.

In the considered case, the diaphragm wall is 26 m long and 80 cm thick. Here, we assume that each wall segment, 6.5 m wide, is stiffened by four pre-stressed anchors. Using all symmetries, in out-of-plane direction, the width of the computational model is 1.625 m. The free water table is located 4 m below the ground surface.

All simulations were run in the real-time domain taking into account consolidation effects, to represent the transient effects in cohesive subsoil. The sequence of excavation/construction stages consists of the in situ stress and pore water pressure generation, wall installation, and then three major excavation stages, until −5 m, −11 m and −16 m. At the −5 m level, the first row of 17-m-long anchors is installed and pre-stressed with a force of 760 kN. The second row of anchors (same length and pre-stress force) is installed at the −11 m level. The assumed total time for all excavation works is about 96 days (resulting excavation rate is 0.167 m/day). The foundation raft is installed 30 days after the final excavation step without any ground supports left to diminish the progressively increasing bending moments. This is a rather conservative assumption as such ground supports may significantly

reduce the maximum bending moments in the diaphragm walls, deflections and maximum crack opening. Starting from that time, three levels of RC floors are constructed and the anchors are progressively cut off. Results of all simulations carried out show that once the foundation raft is installed, bending moments in the wall are decreasing. Therefore, the results for all of these time instances are not important in further structure dimensioning. It has to be emphasised here that each major excavation stage was carried out in three steps (maximum two layers of elements were removed in one computational step). In all simulations, the following HS model parameters for the subsoil were used:

$$E_0^{ref} = 328000 \text{kPa}, \nu = 0.2, E_{50}^{ref} = 20000 \text{kPa}, E_{ur}^{ref} =$$

$$= 70000 \text{kPa}, m = 0.55, \gamma_{0.7} = 5 \cdot 10^{-5}, \phi' = 29^o,$$

$$\psi' = 0^o, c' = 7 \text{ kPa}.$$

A safely estimated value of seepage coefficient $k = 10^{-8}$ m/s was assumed. This parameter plays an important role in dissipation of the excess pore water pressures induced during the excavation stage. The subsoil stress history is represented by a variable $\text{OCR}(z)$ profile resulting from the assumed pre-overburden pressure $q^{POP} = 1300$ kPa. This pressure yields the best fit between the experimental OCR profile, obtained from the CPTU test, and the theoretical one [5]. The corresponding in situ horizontal effective stress profile is estimated using the formula $K_o^{insitu} \approx (1 - \sin \phi')OCR^{0.5}$. In extreme cases, K_o^{insitu} is limited to the value of the passive pressure coefficient K_p.

4.1 Results of analysis using NSO-LST computational strategy

In order to perform the preliminary wall dimensioning, two simulations (Cases A1 and A2), based on the NSO-LST computational strategy, were carried out. In Case A1, a nominal stiffness modulus $E_{cm} = 31000$ MPa for the concrete class C25/30 was used, while in Case A2, a reduced (by 20%) stiffness modulus ($E_{cm} = 25000$ MPa) was used just to check the influence of this parameter.

The envelope of bending moments and the associated membrane forces in the wall, for both Cases A1 and A2, are shown in Fig. 5. As expected, larger moments are obtained for Case A1, but a reduction of the stiffness modulus by 20% yields <7% reduction in the maximum bending moment. A comparison of the envelopes of bending moments in the wall, for Case A1, based on all time instances registered until the last excavation step (labelled as $A1^*$), and on the
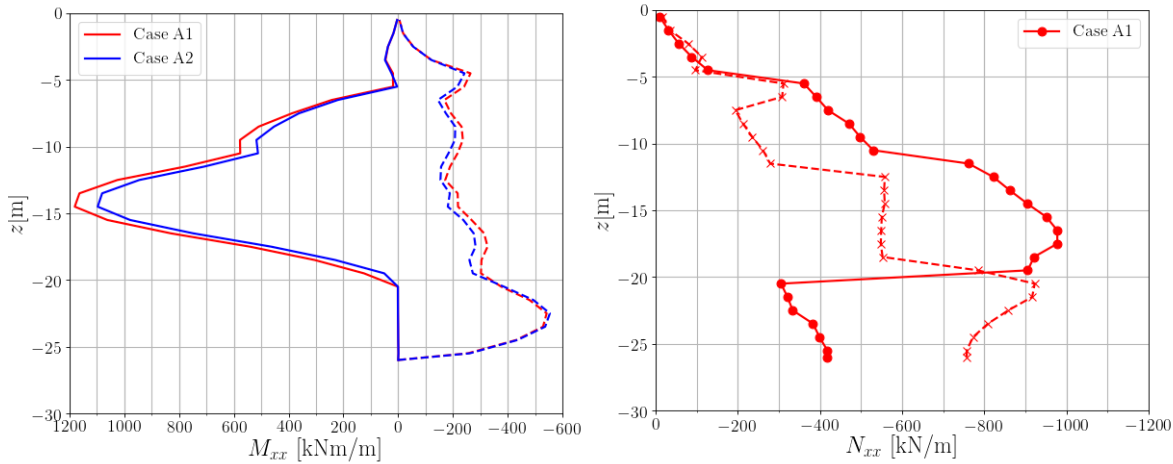
Figure 5: Envelope of characteristic bending moments (Cases A1 and A2) and corresponding membrane forces (Case A1 only) at the time instance when the foundation raft is installed.
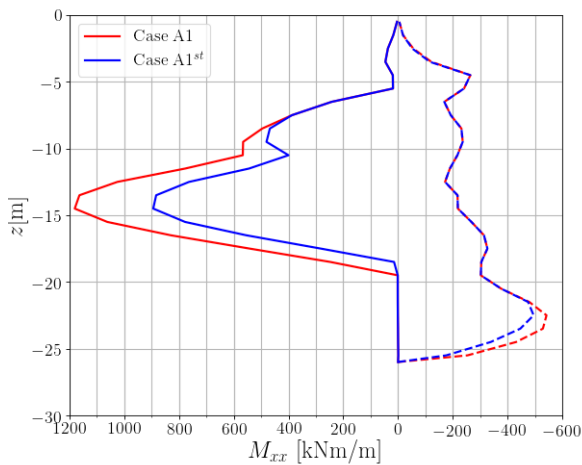

Figure 6: Comparison of characteristic bending moment envelopes (Case A1 only) based on all time instances registered until the last excavation step and then until the time instance at which the foundation raft is installed.

Table 1: Preliminary design of reinforcement in the wall based on the results achieved for Case A1.

Depth range, m	A_{s1}, cm²/m	A_{s2}, cm²/m
−7	12.5	12.5
−10	25.0	12.5
−18	50.0	12.5
−20	12.5	12.5
−26	12.5	18.75

cases are negligible. It is well visible that for the anchored diaphragm walls, protecting deep excavations, foundation rafts should be installed as soon as possible and ground supports should be used as well. Without ground supports, wall deformations increase >30%.

Based on the bending moment envelopes for Case A1 and the associated membrane forces, the following distribution of reinforcement is assumed (see Table 1) (A_{s1} is the reinforcement placed at the internal wall face, while A_{s2} is placed at the external one). This reinforcement will further be verified using non-linear subsoil–non-linear structure (NSO-NST) computational strategy. It has to be emphasised that due to the combined action of the bending moment and the membrane force, in the wall cross-section, but also the large eccentricity (M_{xx}/N_{xx}) case, the characteristic bending moments are amplified by a factor 1.35 (dead load partial factor), to design reinforcement, while the membrane forces are kept unchanged. This assumption leads to conservative dimensioning of reinforcement.
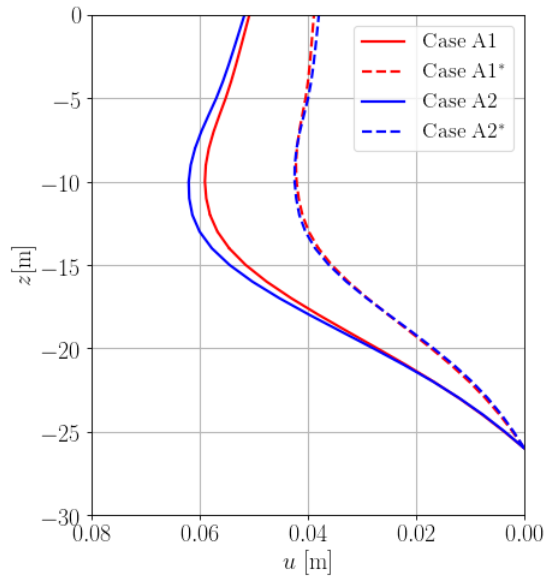
extended set of time instances registered until the foundation raft installation time, is shown in Fig. 6. One can notice that the maximum bending moment can be reduced at best by 24% if ground supports are used. The main role of these supports is to reduce wall movement until the time when the foundation raft is installed. This result is shown here just for a qualitative assessment of the factors influencing the distribution of bending moments in the wall and its deformations. Wall deformations for Cases A1, A1*, A2 and A2* are shown in Fig. 7. As expected, larger deformations (by $\approx 7\%$) are obtained for Case A2, but exclusively at the time instance when the foundation raft is installed. At the time instance corresponding to the last excavation step, differences between the resulting deformations for the two

Figure 7: Comparison of wall deflections (Cases A1 and A2) at the time instance corresponding to the last excavation step (dashed lines) and at the time instance when the foundation raft is installed (solid lines).

4.2 Results of analysis using NSO-NST computational strategy

General rules concerning the conduct of a fully non-linear analysis of subsoil and RC structures are not explicitly specified in EC2, nor in EC7. In the course of the designing process, the two limit states are always analysed, i.e. the ULS and the serviceability limit state (SLS). In the latter one, cracks in the RC structures and deformations, both in the structure and in subsoil, are checked. In the NSO-LST computational strategy, the characteristic stress resultants in the diaphragm wall are selectively increased (only bending moments) by the dead load partial safety factor, equal to 1.35. Then, standard dimensioning procedure is applied to set up the required reinforcement. It is worth mentioning that the soil parameters are not scaled by the partial safety factors to avoid non-physical situations (negative porosity, for instance). Therefore, the same strategy is used for RC structures in which the characteristic values of concrete strength (f_{ck}, $f_{ctk0,05}$) and stiffness E_{cm} are used to calibrate the modified Lee–Fenves model, while the steel reinforcement is characterised by the characteristic strength value f_{yk}. The SLS state, limited to the estimation of deformations, is relatively easy to analyse as all loadings are scaled with the partial safety factor equal to 1.0, the creep phenomenon is activated in the structure, while all parameters in the subsoil and concrete are taken as characteristic (this notion is rather problematic for the subsoil where HS

model parameters are derived from a very limited set of experiments). However, assessment of the maximum crack opening is definitely more complicated.

In the computational FE model (FEM), the diaphragm wall is discretised using shell elements, but no extra interface between the concrete core and the steel reinforcement is introduced. Therefore, strains in concrete and steel are compatible, and such a model is unable to reproduce crack opening in a direct manner. To remedy this serious deficiency, one can assume that the difference between the averaged value of strain in steel and concrete ($\varepsilon_{sm} - \varepsilon_{cm}$) is approximately equal to the value of strain in the steel reinforcement, resulting from the conducted FEM analysis. If we accept this approximation, then standard EC2 procedure for computing maximum crack opening, $w_k = s_{r,max} (\varepsilon_{sm} - \varepsilon_{cm})$, can easily be adopted (see EC2 for more details).

The assessment of ULS state is definitely more problematic. Here, we assume that all parameters in the subsoil and structure are taken as characteristic, or let us say derived for the subsoil, while the computed stress resultants (bending moment and membrane force) at any point of the RC structure are projected on the domain bound by the bending moment–membrane force ultimate interaction curve (see Fig. 8) derived for concrete strength parameters f_{cd} and f_{ctd}, as well as the steel strength f_{yd}. Here, we assume that any stress resultant point (B) having coordinates $\{N_{xx}^B, M_{xx}^B \cdot \tilde{\gamma}\}$ stays inside of the ultimate bending moment–membrane force interaction curve (see Fig. 8). The $\tilde{\gamma}$ value combines the two partial safety factors, i.e. the one corresponding to the dead load (1.35) and the one corresponding to the material one (1.4 for concrete [according to the Polish EC2 version] and 1.15 for steel). The upper bound is $\tilde{\gamma} = 1.35 \cdot 1.4 \approx 1.9$, while the lower bound is $\tilde{\gamma} = 1.35 \cdot 1.15 \approx 1.55$. Here, we will use the upper bound value $\tilde{\gamma} = 1.9$.

As already mentioned, in the NSO-NST computational strategy, the modified Lee–Fenves CPDM is used, in which ageing and creep, compatible with the EC2 standard, is introduced [13, 5]. In the analysed case study, we assume that concrete age, at the beginning of the excavation stage, is approximately 28 days. The following set of material properties for concrete is used in this case study: $E_{cm} = E_{28} = 31000$ MPa, $\nu = 0.2$, $\gamma = 25$ kN/m^3, $f_c = 25$ MPa, $f_{cbo}/f_c = 0.4$, $f_{cbo}/f_c = 1.16$, $\tilde{D}_c = 0.435$ at $\tilde{\sigma}_c/f_c = 1.0$, $G_c = 13.5 *10^{-3}$ MN/m, $f_t = 1.8$ MPa, $\tilde{D}_t = 0.5$ at $\tilde{\sigma}_t/f_t = 0.5$, $G_t = 0.135 *10^{-3}$ MN/m, $s_o = 0.2$, $\alpha_p = 0.2$ and $\alpha_d = 1.0$. Notion of all these parameters is explained in the original paper by Lee and Fenves [3] and in a previous paper by the author [5]. The above set of parameters yields sufficiently good

match with the EC2 uniaxial stress–strain characteristics obtained in the uniaxial compression test. Additional parameters to characterise the creep (for $RH = 0.8$) are as follows: $\phi_o \, \beta(f_{cm})/E_{28} = 1.14*10^{-4}$ MPa^{-1}, $\beta_H = 2000$ days and $s = 0.38$.

The last important aspect concerning modelling RC is related to the estimation of the so-called characteristic length l_{RC}, which should be used to scale the fracture energies in compression G_c and tension G_t in the FEM. For plain concrete, this length is equivalent to the FE size h^e, while in the case of RC structures, its value must carefully be estimated. Here, we assume that in the properly reinforced RC structures, total loss of concrete tensile strength appears at the strain at which steel reinforcement becomes plastic. This yields the following estimate for the l_{RC} value:

$$l_{RC} = \frac{2\,G_f\,E_s}{f_{ctk\,0,05}\,f_{yk}} \tag{16}$$

The above expression is derived assuming a linear decrease in the concrete tensile strength with the axial tensile strain. In the considered case study, the characteristic length $l_{RC} \approx 0.06$ m.

The two cases were analysed at first. In all of them, the NSO-NST computational strategy was used. Case B1 was dedicated to assess the ULS for preliminary design of reinforcement (creep is not activated), while Case B2 was designed to assess the SLS state (with creep).

The resulting bending moment envelopes and the associated membrane force profiles for Case B1 are shown in Fig. 9. In order to obtain the upper bound estimate for the bending moments in the case when ground supports are used and the foundation raft is installed as soon as possible, the two envelopes (B1 and B1∗) are shown in Fig. 10. The maximum bending moment in Case B1 is nearly 930 kNm/m. If we scale it by $\bar{\gamma} = 1.9$, then we will get nearly 1770 kNm/m. This value is larger than the one obtained from Case A1, for which the maximum registered characteristic moment was about 1180 kNm/m (moment used for dimensioning was $1.35*1180 \approx 1590$ kNm/m). So, we see that non-linear computational strategy for $\bar{\gamma} = 1.9$ leads to a more conservative design.

When analysing results of the SLS state (see Fig. 11), we can see that in the best possible case (ground supports are used and foundation raft is installed fast), horizontal deformations of the wall are practically not
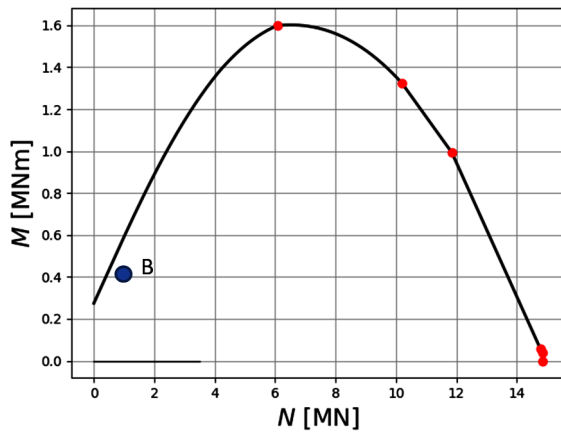

Figure 8: Checking the ULS condition at any point of the structure by projecting the stress resultant pairs $\{N_{xx}, M_{xx} \cdot \bar{\gamma}\}$ on the domain bound by the $N - M$ interaction diagram.
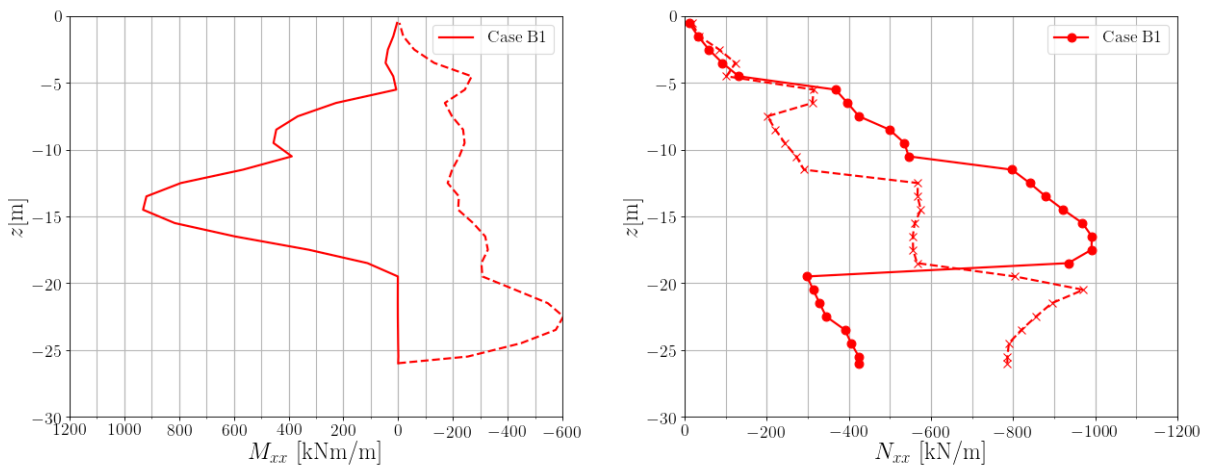

Figure 9: Envelope of characteristic bending moments (Case B1) and corresponding membrane forces at the time instance when the foundation raft is installed.
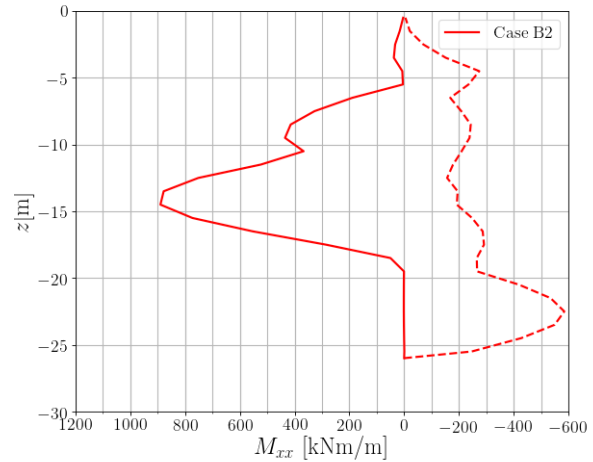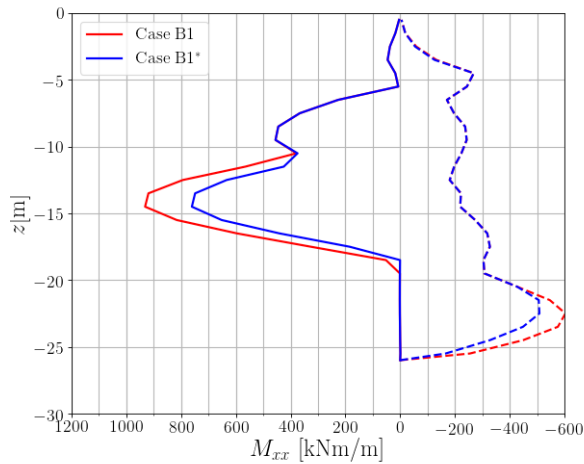
Figure 10: Comparison of characteristic bending moment envelopes based on all time instances registered until the last excavation step (B1*) and then until the time instance at which the foundation raft is installed (B1).
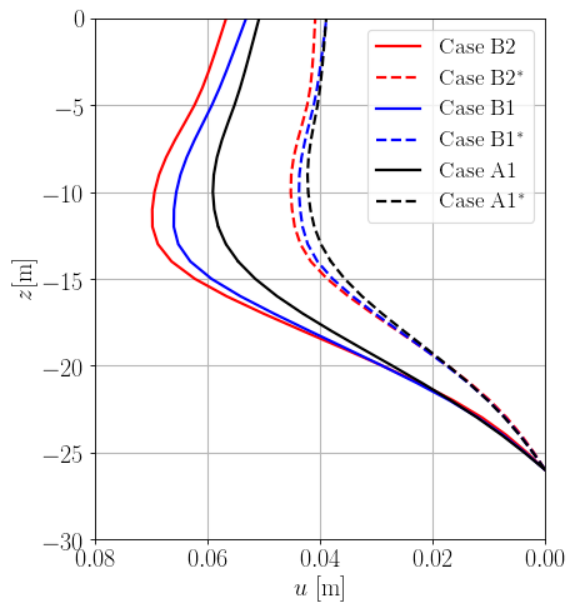

Figure 11: Comparison of wall deflections at the time instance corresponding to the last excavation step (dashed lines) (Cases A1*, B1* and B2*) and at the time instance when the foundation raft is installed (solid lines) (Cases A1, B1 and B2).

Figure 12: Envelope of characteristic bending moments (Case B2) and corresponding membrane forces at the time instance when the foundation raft is installed.

influenced by creep, and small differences, in general, between the two computational strategies are observed. However, in the less-optimal construction technology, these differences become much bigger and creep effects become visible too. The maximum difference in terms of horizontal wall displacements between the Cases B2 and A1 is about 18%.
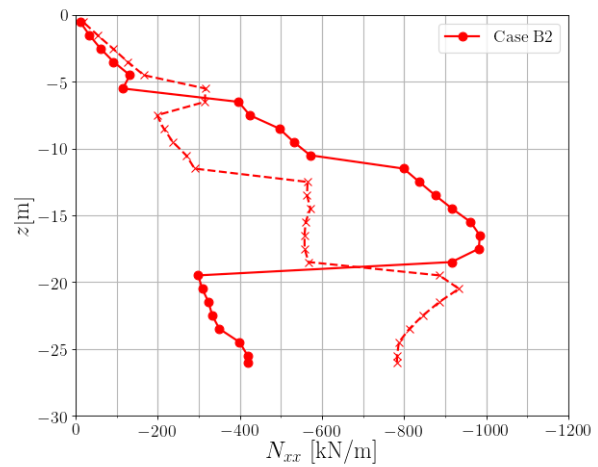
In order to check the maximum crack opening in the zone of the maximum bending moment, the maximum tensile strains have been traced in the steel reinforcement placed at the internal wall face at a depth of 14.5 m, for Case B2 (Fig. 12). The maximum registered value was $\varepsilon_s^{max} = 6.2e-4$. For an assumed net steel cover $c = 10$ cm and equivalent steel bars with diameter $\phi_{eq} = 0.0225$ (mixture of 20/25 mm bars), the $h_{c,ef} = 0.275$ m, $\rho_{p,eff} = 0.0182$ and $s_{r,max} = 0.55$ m (see the chapter on SLS state assessment in EC2). So, the estimated maximum crack opening was $w_k = 0.55 \cdot 6.2e-4 \cdot 1000 = 0.34$ mm. This value should not be >0.3 mm; hence, the major longitudinal reinforcement was increased from 50 cm^2 to $A_{s1} = 57$ cm^2. For this newly designed reinforcement, the maximum registered strain in steel was $\varepsilon_s^{max} = 5.35e-4$,

which yields the maximum crack opening of $w_k = 0.028$ mm.

5 Conclusions

The two computational strategies, i.e. non-linear soil–linear structure (NSO-LST) and non-linear soil–non-linear structure (NSO-NST), were verified based on the selected case study of a diaphragm wall. It was shown that an ad hoc increase in bending moments (in the NSO-LST approach), by the dead load partial safety factor (1.35) may yield insufficient amount of the reinforcement in the wall cross-section. The resulting maximum crack opening may also be unacceptable in that case. On the other hand, the amount of reinforcement resulting from the NSO-NST approach is practically sufficient to satisfy both ULS and SLS states. A consistent conservative approach was proposed to assess the ULS and SLS states in the NSO-NST computational strategies, allowing the combination of fully nonlinear analysis and standards. The developed tools available in the ZSoil code allow for the careful design and checking of all the ULS and SLS conditions in a consistent manner.

References

[1] Obrzud, R., Hartmann, S., Podleś, K. (2016). Selected aspects of designing deep excavations. *Studia Geotechnica et Mechanica*, *38*.

[2] Truty, A., Podleś, S. (2010). Application of Hardening Soil-small model for analysis of soil-structure interaction problems (in Polish). *Czasopismo Techniczne*, *1*, 117-134.

[3] Lee, J., Fenves, G.L. (1998). Plastic-damage model for cyclic loading of concrete structures. *Journal of Engineering Mechanics*, *124*, 892-900.

[4] Lee, J., Fenves, G.L. (2001). A return-mapping algorithm for plastic-damage models: 3-D and plane stress formulation. *IJNME*, *50*, 487-506.

[5] Truty, A. (2016). Elastic-plastic damage model for concrete. Technical Report, ZSoil.PC 160102, January.

[6] Schanz, T. (1998). Zur Modellierung des mechanischen Verhaltens von Reinbungsmaterialien. In *Mitt. Inst. für Geotechnik 45*. Universitat Stuttgart, Stuttgart.

[7] Schanz, T., Vermeer, P.A., Bonier, P.G. (1999). Formulation and verification of the Hardening Soil Model. In *Beyond 2000 in Computational Geotechnics*. Balkema, Rotterdam.

[8] Benz, T. (2006). Small-strain stiffness of soils and its numerical consequences. Ph.D. Thesis, University of Stuttgart.

[9] Truty, A., Obrzud, R. (2015). Improved formulation of the Hardening Soil model in the context of modeling the undrained behavior of cohesive soils. *Studia Geotechnica et Mechanica*, *37*, 61-68.

[10] Obrzud, R., Truty, A. (2010). The hardening soil model: A practical guidebook. Technical Report Technical report ZSoil.PC 100701, ZACE Ltd, Lausanne.

[11] Lubliner, J., Oliver, J., Oller, S., Oñate, E. (1989). A plastic-damage model for concrete. *International Journal of Solids and Structures*, *25*(3), 299-326.

[12] Oller, S., Oñate, E., Oliver, J., Lubliner, J. (1990). Finite element nonlinear analysis of concrete structures using a plastic-damage model. *Engineering Fracture Mechanics*, *35*, 219-231.

[13] Truty, A., Zimmermann, Th. (2015). Modified Lee-Fenves plastic-damage model for concrete. In *Numerics in Geotechnics*. Elmepress Ltd., Lausanne, Switzerland.

[14] Havlásek, P. (2014). Creep and shrinkage of concrete subjected to variable environmental conditions. Ph. D. Thesis, Czech Technical University in Prague.

[15] Truty, A., Podleś, K. (2016). Influence of diaphragm wall installation in overconsolidated sandy clays on in situ stress disturbance and resulting deformations. *Annals of Warsaw University of Life Sciences – SGGW Land Reclamation*, *48*, 243-253.